INVESTIGATING THE SOURCE(S) OF DARK SAND IN THE WESTERN MEDUSAE FOSSAE FORMATION, MARS. D. M. Burr[1] , R. E. Jacobsen[2], C. E. Viviano[3], T. I. Michaels[4] and M. Chojnacki[5], [1]Northern Arizona University (Devon.Burr@nau.edu), [2]University of Tennessee, Knoxville. [3]JHU Applied Physics Laboratory, Laurel, MD. [4]Southwest Research Institute, Boulder, CO. [5]Planetary Science Institute, Tucson, AZ

Introduction: Sand is globally distributed and moving on Mars [1-12]. Dune morphologies imply saltation, during which grains move downwind in a series of hops. With the high threshold wind velocities on Mars [13], the impact of these saltating grains likely comminutes them to sub-sand sizes [14-16]. Thus, the discovery of pervasive sand movement highlights the decades-old question [see summary in 17] as to source(s) of this globally-distributed sand.

Local sources – such as Valles Marineris wall rock [18-20], the olivine bedrock at Nili Fossae [21, 22], and the basal unit of North Polar Layered Deposits [23, 24] -- obviate the need for long-distance sand transport. However, these sources are confined to tectonovolcanic or polar regions, whereas sand is distributed throughout the intercrater plains and other mid-latitude locales [1,2]. Although some craters yield sand from low-albedo strata in their walls, the evidence for sand leaving craters is questionable and the origin of those dark layers is uncertain [25-27].

A longstanding hypothesis for an origin of Mars sand is as volcaniclastic deposits [25-28], including explosive (ignimbrite) sediments and comminuted effusive (lava) materials. In this work, we test the volcaniclastic hypothesis in the western region of the Medusae Fossae Formation (MFF) (*Fig. 1*).

Background: The MFF is an extensive, light-toned, layered and abraded deposit that stretches ~75 degrees along the highland-lowland boundary (HLB). An ignimbrite origin for the formation is supported by yarding morphology [29-33], low loss tangents from radar [34, 35], and modeling of ash dispersal from adjacent volcanic edifices [36-38]. Although the specific source for the MFF is still under investigation, an ignimbrite interpretation is consistent with evidence for explosive volcanism on Mars [39,40].

Ignimbrites are comprised of a wide range of grain sizes, including dust and sand [41]. The western MFF (wMFF; Fig. 1) exhibits numerous dark sand dunes (*Fig. 1, inset*) and a mantle of dust [42]. Based on evidence for recent mobility [36], we hypothesize that MFF abrasion liberates sediment and concentrates sand to form the observed dark dunes. In addition to testing the MFF itself, we test three other potential sources for western MFF sand: 1) Cerberus plains lavas, 2) explosive deposits on the Elysium Mons edifice, and 3) the southern highlands.

Methodology: Our methodology is to map sand deposits in the wMFF, to use deposit morphology to infer emplacement wind directions, and to compare the deposit locations and inferred wind directions with mesoscale atmospheric modeling results to determine the most likely sand source(s). For an independent dataset, we compare spectra from the wMFF sand and the four possible source regions.

1. Mapping. We mapped optically dark sand in the blended mosaic of Context Camera [CTX] images (res. 6 m/px; [43]). Because the western MFF sand appears bright in both day and nighttime thermal imaging, we also used day and nighttime data from the Thermal Emission Imaging System [THEMIS; 44] for mapping. Dark sands were delineated as polygons on the CTX mosaic at the mapping scale of 1:25,000.

2. Morphological analysis. Mapped deposits were examined for wind direction indicators (e.g., slip face orientations) in the CTX mosaic and available images from the High Resolution Imaging Science Experiment [HiRISE; 45]. From the uni- and bidirectional indicators, we calculated geospatial statistics (*Fig. 2*).

3. Modeling. To predict sand location and wind direction, we will use the Mars Regional Atmospheric Modeling System [MRAMS; 46] with boundary conditions from the Mars Global Climate model [47]. Inputs will include regional topography over the wMFF and possible external sand source regions. Initial runs will model present-day orbital/axial state, consistent with low dust cover in some locations. Based on lack of recent observable movement [9], we will also model other orbital/axial states.

4. Compositional comparison. As an independent assessment, we will use data from the Compact Reconnaissance Imaging Spectrometer for Mars (CRISM; [48]) to quantify compositional similarity between wMFF sand and all potential sand sources. Spectra will be analyzed using band depths and centers at 2- and 1-μm, respectively [see 49].

Results. Our mapping results show sand is clustered within Aeolis Chaos (a ~1-km-deep depression), found on Zephyria Plana, and scattered in the interplanar trough (*Fig. 2*). Morphological wind direction indicators suggest local topographic control. Preliminary spectral analysis shows an olivine/pyroxene continuum with the wMFF at an extremum (*Fig. 3*).

Conclusions and future work: The clustering of sand in Aeolis Chaos and evidence for local topographic control elsewhere both suggest that sand is not traveling far within the wMFF, either due to topographic barriers or to comminution to sub-sand sizes.

The extremum spectral position of wMFF bedrock suggests the effectiveness of spectroscopy in determining wMFF sand source(s). In future work, we will 1) model predicted sand locations and wind directions, 2) compare those predictions to our mapping and morphological analyses, and 3) complete our ongoing CRISM analysis of the study area and potential source regions. We will then evaluate these multiple datasets will to identify the most likely source region(s) for the observed dark sand in the wMFF.

Acknowledgments: This work is supported by the Mars Data Analysis Program.

References: [1] Hayward R.K. et al. (2007) *JGR Planets*, E11007. [2] Hayward R.K. et al. (2014) *Icarus* 230, 38-46. [3] Bourke M.C. et al. (2008) *Geomorph.* 94, 247-255. [4] Silvestro S. et al. (2010) *GRL* 37, L20203. [5] Silvestro S. et al. (2011) *GRL*, 38, L20201. [6] Chojnacki M. et al. (2011) *JGR Planets* 116, E00F19. [7] Bridges N.T. et al. (2012) *Nature*, 485, 339-342. [8] Bridges N.T. (2012) *Geology*, 40, 31-34. [9] Chojnacki M. et al. (2019) *Geology,* doi.org /10 .1130 /G45793.1. [10] Sullivan R. et al. (2008) *JGR* 113, E06S07. [11] Ewing R.C. et al. (2017) *JGR Planets*, 122, 2544-2573. [12] Bridges N.T. and Ehlmann B. L. (2018) *JGR Planets,* 123, 3-19. [14] Kok J.F. et al. (2012) *Rep. Prog. Phys.* 75, 10690. [14] Sagan, C. et al. (1977) *JGR*, 82, 4430-4438. [15] Greeley R. and Kraft M.D. (2001) *LPS XXXII,* abs 1839. [16] Sullivan R. et al. (2005) *Nature*, 436, 58-61. [17] Melosh H.J. (2011) Planetary Surface Processes, Cambridge University Press. [18] Roach L.H. et al. (2010) *Icarus*, 206, 253-268. [19] Chojnacki M. et al. (2014) *Icarus*, 232, 187-219. [20] Chojnacki M. et al. (2014) *JGR*, 116, E00F19. [21] Mangold N. et al. (2007) *JGR*, 112, E08S04. [22] Ehlmann, B.L. et al. (2010) *GRL*, 37, L06201. [23] Langevin Y. et al. (2005) *Science*, 307, 1584-1586. [24] Fishbaugh K.E. (2007) *JGR*, 112, E07002. [25] Fenton. L.K. et al. (2003) *JGR*, 108, p. 5129. [26] Fenton L.K. (2005) *JGR*, 110, 1-27. [27] Tirsch D. et al. (2011) *JGR,* 116, E03002. [28] Edgett K.S. and Lancaster N. (1993) *J Arid Env.,* 25, 271-297. [29] Ward, A.W. (1979), *JGR*, 84, 8147-8166. [30] Scott, D.H. and Tanaka K.L. (1986) *USGS SIM*, I-1802-A. [31] Wells G.L. and Zimbelman J.R. (1997) in Arid Zone Geomorphology, John Wiley & Sons. [32] Mandt K.E. (2008) *JGR,* 113, E12011. [33] Mandt K. E. (2009) *Icarus*, 204, 471-477. [34] Watters T.R. et al. (2007) *Science*, 318, 1125-1128. [35] Carter L.M. et al. (2009) *Icarus* 199, 295-302. [36] Keber L. and Head J.W. (2010) *Icarus,* 216, 669-684. [37] Kerber L. et al. (2012) *Icarus* 216, 212-220. [38] Kerber L. et al. (2012) *Icarus,* 219, 358-381. [39] Tanaka K.L. et al. (1992) in Mars, p. 345-382. [40] Michalski J. R. and Bleacher, J.E. (2013) *Nature* 502, 47-52. [41] Sparks R.S.J. (1976) *Sed.* 23, 147-188. [42] Ruff S.W. and Christensen P.R. (2002) *JGR*, 107, p. 5127. [43] Dickson. J.L.et al.(2018) *LPS IL*, abs. 2480.[44] Christensen P.R. (2004) *SSR* 110, 85-130. [45] McEwen A.S. et al. (2007) *JGR* 112, E05S02. [46] Rafkin S.C. R. et al. (2001) *Icarus*, 51, 228-256. [47] Haberle, R.M. et al. (2003) *Icarus* 161, 66-89. [48] Murchie S. et al. (2007) *JGR*, 112. [49] Viviano C.E. et al. (2019), *Icarus*, 328, 274-286.

Fig. 1. The wMFF (block box) and three possible external sand source regions. Inset: dark sand (left) with scours (circles) as one type of wind direction indicator.

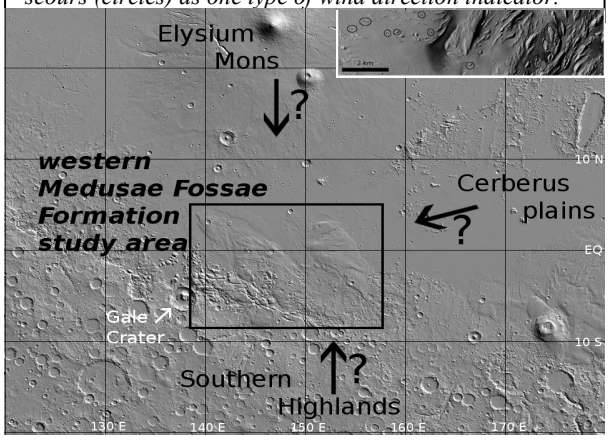

Fig. 2. Mapped sand deposits with emplacement wind directions inferred from six types of wind indicators.

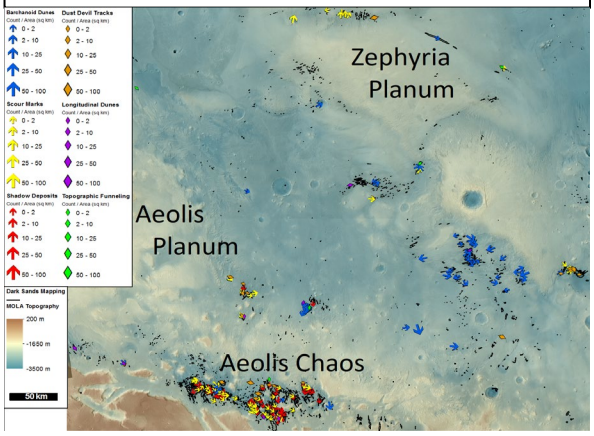

Fig. 3.CRISM Band II (2-μm) depth vs. Band 1 (1-μm) center for possible sand source regions, with wMFF at an extremum.